

Time-dependent wave-packet treatment of the $\text{Si}^{4+} + \text{He}$ collision

Nathalie Vaeck

Laboratoire de Chimie Physique Moléculaire, CP 160/09 Université Libre de Bruxelles, 50 Avenue F. Roosevelt, B-1050 Bruxelles, Belgium

Marie-Christine Bacchus-Montabonel

Laboratoire de Spectrométrie Ionique et Moléculaire, UMR 5579, CNRS et Université de Lyon I, 43, Boulevard du 11 Novembre 1918, 69622 Villeurbanne Cedex, France

Ezinvi Baloïtcha and Michèle Desouter-Lecomte*

*Laboratoire de Chimie Physique, UMR 8000, Université de Paris Sud, 91405 Orsay Cedex, France
and Département de Chimie, Université de Liège, Institut de Chimie B6, Sart-Tilman, B-4000, Liège 1, Belgium*

(Received 31 August 2000; published 12 March 2001)

The collisional system $\text{Si}^{4+} + \text{He}$ has been studied over a range of mean relative ion kinetic energy going from 10^{-2} to 10^2 eV/amu. In the low-energy range, a time-dependent wave-packet approach is used both in the diabatic and the adiabatic representation using two different propagator techniques. The agreement between the two sets of results assess the accuracy of the present numerical approach. Above 2.5 eV/amu., a semiclassical eikonal calculation is performed, which includes the Coriolis couplings. Finally, the rate constant is calculated and compared with the other theoretical data as well as with the experimental value of [Fang and Kwong, Phys. Rev. A **59**, 342 (1999)]. The present results confirm the order of magnitude of previous theoretical values.

DOI: 10.1103/PhysRevA.63.042704

PACS number(s): 34.70.+e, 31.30.Gs

I. INTRODUCTION

Since the pioneering theoretical work on the charge transfer between atoms and ions by Bates and Moiseiwitsch in 1954, silicon ions have been often studied because of their importance in the modelization of astrophysical plasmas [2]. The relevant collisional systems where mainly Si^{n+} ($n = 2 - 4$) + H and He. A complete discussion of the astrophysical implications of the $\text{Si}^{4+} + \text{He}$ reaction has, for example, been given in Ref. [3]. Although, these systems have already received a lot of attention, a renewal of interest has emerged in connection with the recent experiment of Fang and Kwong [1] providing among the first experimental data on a charge-transfer rate coefficients at low temperatures.

Four different dynamical calculations have been performed on the collisional system $\text{Si}^{4+} + \text{He}$. Butler and Dalgarno [4] used the Landau-Zener method together with empirical potentials. Opradolce *et al.* [5] investigated the same system with a close-coupled approach and a molecular quantum calculation based on model potentials adjusted to asymptotical energy differences. The results of Stancil *et al.* [3] were obtained by the close-coupled quantum method and fully *ab initio* molecular calculations performed with the spin-coupled valence bond method [7]. Finally, Bacchus-Montabonel and Ceyzeriat [6] used a different *ab initio* method and a semiclassical dynamical approach. In addition to the rather different static and dynamical approaches, two calculations [5,6] included Coriolis couplings between Σ and Π states as well as electron-translation effects. Both effects have been found negligible at low collision energy. However, discrepancy persists among these works mostly at low

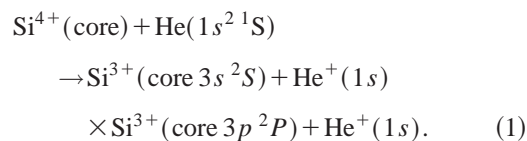
energy. Moreover, the recent measurement [1] performed by Fang and Kwong using a laser-induced plasma ion source and ion storage gives rise to a charge-transfer rate coefficient for the $\text{Si}^{4+} + \text{He}$ reaction two orders of magnitude smaller than the available theoretical values.

The purpose of this paper is to investigate the charge exchange $\text{Si}^{4+} + \text{He}$ reaction in a large range of energy, first at low energy using the time-dependent approach developed recently to solve the close coupling equations [8], second, at higher energy using a semiclassical approach that includes Coriolis effects. The calculation of the rate constant is performed and compared with the theoretical data as well as with the value of Fang and Kwong.

The time-dependent approach is strictly equivalent to the standard time-independent close-coupling approach used generally for scattering problems. However, the time-dependent methods provide clear and direct physical insight into the dynamics in much the same way as classical mechanics. The collision matrix elements are extracted by Fourier transforming the time signal obtained from a wave packet stored in the postcollisional region. The radial time-dependent wave functions are transformed to the scattered part of the stationary wave functions. We check the efficiency of resolving the coupled equations in the diabatic or in the adiabatic basis set.

II. AB INITIO CALCULATIONS

In our paper, two reaction channels are considered:



*Author to whom correspondence should be addressed.

TABLE I. Position of the avoided crossing points (R_x), adiabatic potential-energy differences (ΔE_x^a) and height of the radial coupling matrix elements ($P_{\alpha\beta}$) at the avoided crossing.

Molecular states	R_x (a.u.)	ΔE_x^a (eV)	$ P_{\alpha\beta} $ (a.u.)	References
EC - $3p\ ^1\Sigma^+$	7.0	0.112		[4]
	6.975	0.244		[5]
	7.0	0.344	2.4	[3]
	6.95	0.365	2.38	[6]
	7.00	0.309	2.604	This paper
$3p\ ^1\Sigma^+ - 3s\ ^1\Sigma^+$	4.0	2.1		[4]
	4.5	2.46		[5]
	4.6	3.385	0.8	[3]
	4.45	3.417	0.74	[6]
	4.5	3.121	0.787	This paper
EC - $3s\ ^1\Sigma^+$	2.8	25.641	0.320	This paper

The $3d\ ^2D$ state of Si^{3+} is located asymptotically 0.024 a.u. below the entrance channel that corresponds roughly to a crossing at $R > 120$ a.u. At this internuclear distance, the transition will be totally nonadiabatic; the system follows the diabatic curve of the entrance channel with no significant effect on the results of the collision. This assumption has been verified using a semiclassical approach that shows that for a kinetic energy of 122.5 eV/amu the state-selected electron transfer to the 2D state is about 7.73×10^{-20} cm², i.e., totally negligible.

The quantum chemical calculation performed in this paper using the code MOLPRO [9] is similar to that of Bacchus-Montabonel and Ceyzeriat [6]. A pseudopotential has been used to describe the core orbitals $1s^2 2s^2 2p^6$ of the Si atom [10]. The Gaussian primitives of the $9s7p2d$ basis of McLean and Chandler [11] have been used and the contraction coefficients optimized on the $\text{Si}^{3+}(3s)\ ^2S$ state for the s functions, on the $\text{Si}^{2+}(3s3p)\ ^3P$ state for the p functions, and on the $\text{Si}^{2+}(3s3d)\ ^3D$ state for the d functions. The corresponding contraction coefficients are given in Ref. [12]. Extra f orbitals from the correlation-consistent polarized cc pVTZ basis of Dunning [13] have been added with no contraction applied. The standard VTZ basis set of Dunning without contraction has been used for the He atom [14]. The molecular orbitals have been optimized in a state-average complete active space self-consistent field (CASSCF) calculation [15,16] on the first three $^1\Sigma^+$ states followed by a calculation multireference configuration-interaction (MRCI) calculation. The $3s$, $3p$, and $3d$ orbitals of Si^{3+} and the $1s$ orbital of He were chosen as active orbitals.

The adiabatic electronic wave functions $\{a_\alpha\}$ obtained in this calculation have been used to determine the different coupling matrix elements between the collision channels. The radial matrix elements

$$P_{\alpha\beta} = \langle a_\alpha | \frac{\partial}{\partial R} | a_\beta \rangle \quad (2)$$

have been calculated using a numerical differentiation method with three points using a step of 0.0012 a.u. The

$\langle a_\alpha | \partial^2 / \partial R^2 | a_\beta \rangle$ elements used in the adiabatic representation have been computed from the following equation [17,18]:

$$Q_{\alpha\beta} = \langle a_\alpha | \frac{\partial^2}{\partial R^2} | a_\beta \rangle = \frac{\partial}{\partial R} \langle a_\alpha | \frac{\partial}{\partial R} | a_\beta \rangle + \sum_\gamma \langle a_\alpha | \frac{\partial}{\partial R} | a_\gamma \rangle \langle a_\gamma | \frac{\partial}{\partial R} | a_\beta \rangle. \quad (3)$$

At higher energy, the Coriolis couplings

$$L_{\alpha\beta} = \langle a_\alpha | iL_y | a_\beta \rangle \delta(\Lambda_\alpha, \Lambda_\beta \pm 1), \quad (4)$$

have been included in the semiclassical calculations. They have been calculated as the matrix element of the iL_y operator in a state-average CASSCF calculation, which includes the first three $^1\Sigma^+$ states and the first $^1\Pi^+$ state. These couplings, except for the signs, are very similar to those shown in Ref. [6].

The *ab initio* parameters (the positions, the energy differences and the height of the radial coupling matrix elements, $P_{\alpha\beta}$, at the avoided crossing points) are given in Table I and compared with the other theoretical values. From the table, it is clear that the last three calculations (Stancil *et al.*, Bacchus-Montabonel and Ceyzeriat [3,6], and the present paper) show very similar parameters despite the difference in the *ab initio* methods.

III. NONADIABATIC AND ADIABATIC WAVE PACKET DYNAMICS

The unitary matrix \mathbf{F} transforming the adiabatic representation into the diabatic representation has been obtained by solving the equation

$$\frac{\partial}{\partial R} \mathbf{F} + \mathbf{P}\mathbf{F} = 0, \quad (5)$$

where the \mathbf{P} matrix contains the radial coupling matrix elements (2). The diagonal and nondiagonal diabatic potential-energy curves are given in Fig. 1. When compared with the

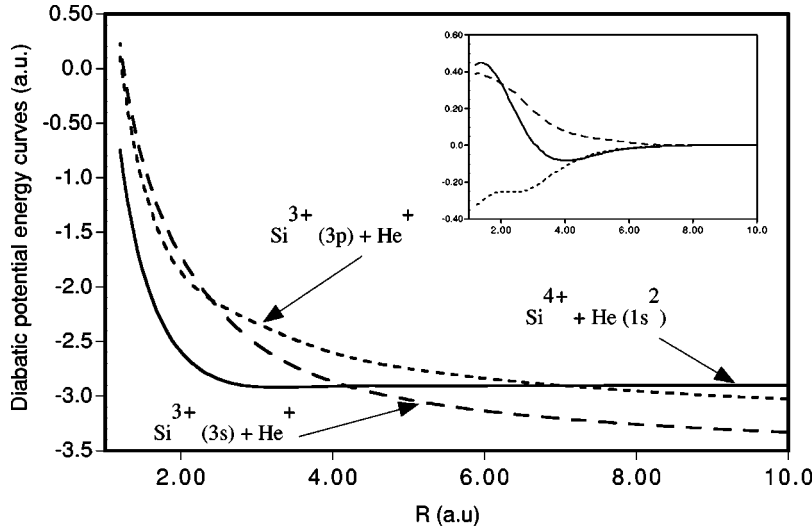


FIG. 1. Diagonal diabatic potential-energy curves with the origin of the electronic coordinates at the center of mass of the nuclei. The inset shows the corresponding nondiagonal diabatic potential matrix elements.

diabatic curves shown by Stancil *et al.* [3], the main difference is a crossing between the $3s$ $^1\Sigma^+$ and the $3p$ $^1\Sigma^+$ states at 2.396 a.u. The two other crossings take place at 4.196 a.u. and 7.007 a.u. between the entrance channel and the $3s$ $^1\Sigma^+$ states and between the entrance channel and the $3p$ $^1\Sigma^+$ states, respectively.

The theoretical model used to solve the time-dependent Schrödinger equation

$$i\hbar \partial [R\Psi(\vec{r}, \vec{R}, t)] / \partial t = \bar{H} [R\Psi(\vec{r}, \vec{R}, t)], \quad (6)$$

where \bar{H} , the total transformed Hamiltonian ($\bar{H} = RHR^{-1}$) in the diabatic representation, has been described in detail by Vaeck *et al.* [8]. Here are given the main differences and similarities between the diabatic and adiabatic dynamics. In summary, the wave function corresponding to the entry channel i is given by the superposition

$$\Psi_i^K(\vec{r}, \vec{R}, t) = \frac{1}{R} \sum_{\alpha\Lambda} \chi_{\alpha\Lambda}^K(R, t) \eta_{\alpha\Lambda}(\vec{r}; R) Y_{\Lambda}^K(\theta, \phi), \quad (7)$$

where K is the total angular momentum with Λ its projection on the internuclear axis. The nuclear wave functions are the product of an angular part, Y_{Λ}^K , and a radial part that contains the entire time dependence $\chi_{\alpha\Lambda}^K$. The electronic wave functions $\eta_{\alpha\Lambda}$ can be expressed in the adiabatic ($\eta_{\alpha\Lambda} = a_{\alpha\Lambda}$) or in the diabatic ($\eta_{\alpha\Lambda} = d_{\alpha\Lambda}$) representation. The corresponding time-dependent functions $\chi_{\alpha\Lambda}^K(R, t) = A_{\alpha\Lambda}^K(R, t)$ or $\chi_{\alpha\Lambda}^K(R, t) = D_{\alpha\Lambda}^K(R, t)$ are a solution of the coupled equations

$$i\hbar \frac{\partial \chi_{\alpha\Lambda}^K(R, t)}{\partial t} = \sum_{\beta\Lambda'} \mathbf{H}_{\alpha\Lambda, \beta\Lambda'}^K \chi_{\beta\Lambda'}^K(R, t). \quad (8)$$

The \mathbf{H}^K matrix is written

$$\mathbf{H}^K = T_R \mathbf{1} + \mathbf{E}^a + \frac{K(K+1) - 2\Lambda^2}{2\mu R^2} \mathbf{1} \\ \mp \frac{\sqrt{(K \mp \Lambda)(K \pm \Lambda + 1)}}{\mu R^2} \mathbf{L} - \frac{1}{2\mu} \left[\mathbf{Q} + 2\mathbf{P} \frac{\partial}{\partial R} \right] \quad (9)$$

in the adiabatic representation or

$$\mathbf{H}^K = T_R \mathbf{1} + \mathbf{H}^d + \frac{K(K+1) - 2\Lambda^2}{2\mu R^2} \mathbf{1} \\ \mp \frac{\sqrt{(K \mp \Lambda)(K \pm \Lambda + 1)}}{\mu R^2} \mathbf{K}^d \quad (10)$$

in the diabatic one. T_R is the nuclear kinetic-energy operator, $T_R = -\hbar^2/2\mu \partial^2/\partial R^2$. \mathbf{E}^a is the diagonal matrix of the adiabatic energies and \mathbf{H}^d and \mathbf{K}^d are, respectively, the matrices of the electronic Hamiltonian and of the Coriolis coupling in the diabatic basis set. The radial coupling \mathbf{P} , \mathbf{Q} , and \mathbf{L} matrices have been defined in Eqs. (2), (3), and (4). The choice of the sign is determined by the sign in Eq. (4). In the present quantum-mechanical calculation, the Coriolis coupling has been neglected so that only Σ states ($\Lambda=0$) are accounted for.

The radial wave function for the initial state ($\alpha=i$) at time $t=0$ is given by a Gaussian wave packet

$$\chi_{\alpha=i}^K(R, t=0) = \frac{1}{(\pi\sigma_R^2)^{1/4}} \exp(-ik_0R) \exp - \frac{1}{2} \left(\frac{R-R_0}{\sigma_R} \right)^2, \quad (11)$$

where $k_0 = \sqrt{2\mu\varepsilon_0}/\hbar$ is the wave number corresponding to the mean relative kinetic energy ε_0 in the entrance channel, R_0 is the initial position of the Gaussian wave packet, and σ_R fixes its width at half maximum in the coordinate domain ($\Gamma_R = 2.354\sigma_R$).

Equation (8) is solved by propagating the wave packet on the three $^1\Sigma^+$ states ($\Lambda=0$) using the split-operator technique in the diabatic representation [19,20] and the more CPU time consuming Chebyshev scheme in the adiabatic basis set [21]. The difference comes from the structure of the \mathbf{H}^K matrix in the two representations. The Chebyshev method only requires the computation of $\bar{H}\Psi$ and is then able to account for any kind of differential operators. The split-operator formalism applies the potential terms in a discrete variable representation and the kinetic terms in the cor-

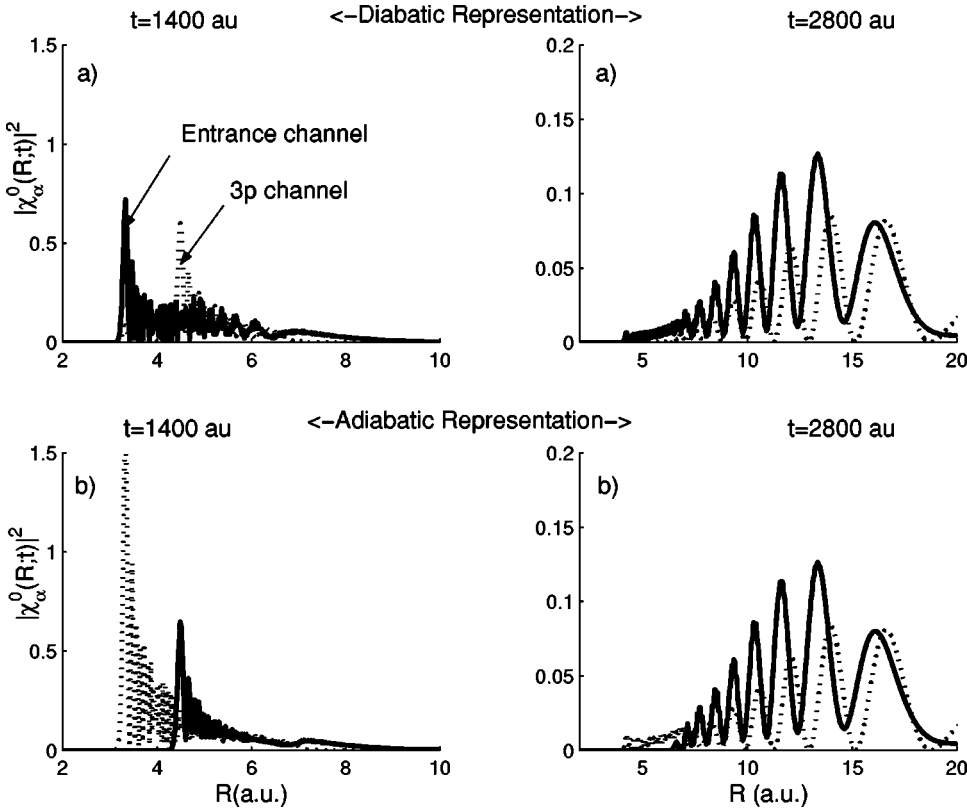


FIG. 2. Time evolution of the components of the wave packet on the $3p\sigma^1\Sigma^+$ and on the entrance channel for $K=0$. The relative kinetic energy of the incident Si^{4+} ion is 1.62 eV/amu. Two schemes of propagation have been used: the split-operator technique in the diabolic representation and the Chebyshev method in the adiabatic representation (see text).

responding finite basis representation. In Cartesian coordinates, this is possible only if the kinetic operator is simply $\partial^2/\partial R^2$ as in the diabolic representation. The time evolution of the wave packet at $K=0$ in the two representations is illustrated in Fig. 2 for a mean kinetic energy of 1.62 eV/amu. After 1400 a.u. of time, the wave packet is already on the way out of the collision. It is split on the entrance channel and the $3p^1\Sigma^+$ channel, the $3s^1\Sigma^+$ channel being neglected. While the two propagation schemes using the diabolic and the adiabatic representations give different results at $t=1400$ a.u., exactly the same results are obtained in the asymptotic region at $t=2800$ a.u. assessing the numerical convergence of the present calculations.

The structures appearing in the wave packet after the crossing of the interaction zone reflect the Stueckelberg interferences arising from the intersections of the different collisional channels. The same effect has been found by Stancil *et al.* [3] to be at the origin of the pronounced oscillatory structure in the total electron-transfer cross section. The same behavior was already mentioned by Zygelman *et al.* [22,23] for the $\text{N}^{4+} + \text{H}$ system.

In order to extract the S -matrix elements, the radial time-dependent nuclear wave function is transformed to the scattered part of the energy-dependent stationary functions

$$B_{\beta}^K(R_{\infty}, E) = \frac{1}{2\pi\hbar} \int_0^{\infty} e^{iEt/\hbar} \chi_{\beta}^K(R_{\infty}, t) dt, \quad (12)$$

where $\chi_{\beta}^K(R_{\infty}, t)$ is the amplitude of the wave packet in the channel β in the asymptotic region.

For each channel β , the elements of the S matrix are given by the relation [8]

$$S_{\beta,i}^K(E) = -\frac{\hbar^2 k_i(E)}{\mu} \frac{\sqrt{k_{\beta}(E)}}{\sqrt{k_i(E)}} \frac{B_{\beta}^K(R_{\infty}, E)}{\exp[ik_{\beta}(E)R_{\infty}]g[k_i(E)]}, \quad (13)$$

where

$$g(k) = \{2\pi\}^{-1/2} \int \chi_{\alpha=i}(R, 0) \exp(ikR) dR \quad (14)$$

and $k_{\beta}(E) = [2\mu(E - E_{\beta})]^{1/2}/\hbar$.

The amplitude of the wave packet in the asymptotic region, $\chi_{\beta}^K(R_{\infty}, t)$, is therefore the only requirement to extract the collision parameters. Figure 3 shows the $\chi_{\beta}^K(R_{\infty}, t)$ functions obtained using the two propagation schemes in the diabolic and the adiabatic representations. The equivalence between the two calculations is excellent. The adiabatic representation circumvents the need for diabaticization, which may be a problem in polyatomic systems. However, the CPU time for the propagation is very different in the two basis sets. It can be carried out by the fast split-operator algorithm in the diabolic case but not in the adiabatic case for which the Chebyshev algorithm must be used.

The time-dependent probabilities of occupation of the different electronic states

$$P_{\alpha\Lambda}^K(t) = \int_0^{\infty} |\chi_{\alpha\Lambda}^K(R, t)|^2 dR \quad (15)$$

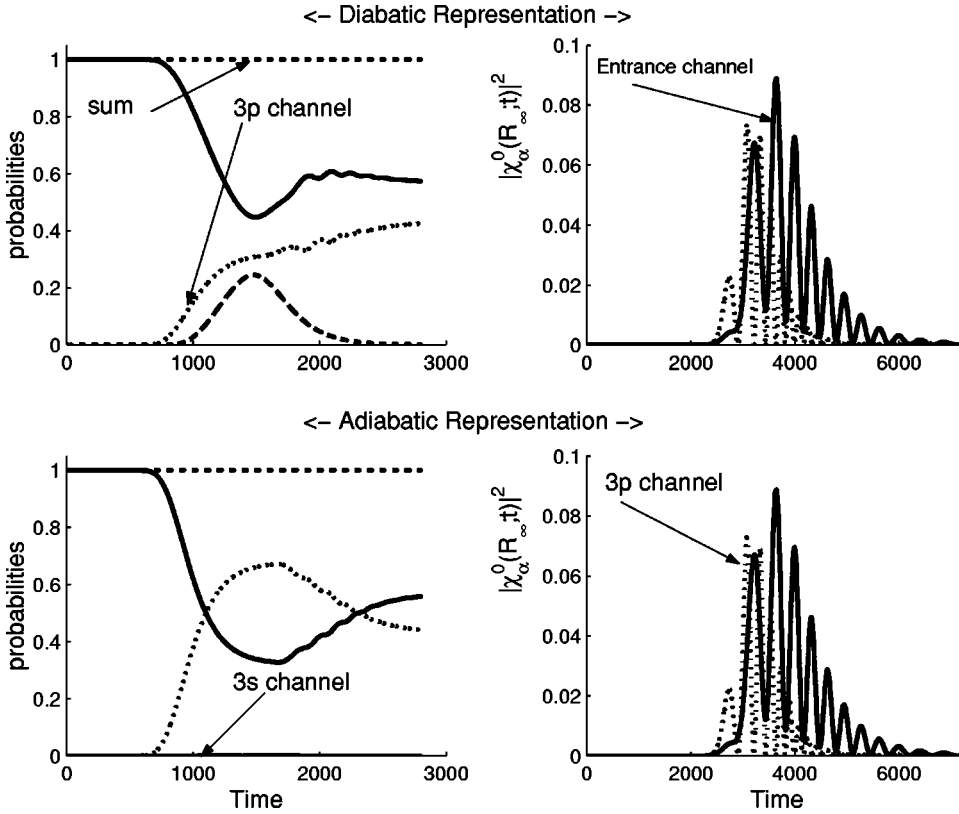


FIG. 3. Square modulus of the wave packet for $R \rightarrow \infty$ as a function of time and time-dependent probabilities of occupation of the first three $^1\Sigma^+$ states for $K=0$. The relative kinetic energy of the incident Si^{4+} ion is 1.62 eV/amu.

are also shown in Fig. 3 for $K=0$ and a relative kinetic energy of the incident Si^{4+} ion of 1.62 eV/amu. Contrary to elements of the S matrix, the probabilities as a function of time depend on propagation parameters and therefore these quantities are of no use for comparison with experimental data.

The expression of the state-selective electron-transfer cross section is given by

$$\sigma_{\beta,i}(E) = \frac{\pi}{(2L_i+1)k_i^2(E)} \sum_K \sum_{\Lambda\Lambda'} (2K+1) \times |i[S_{\beta\Lambda',i\Lambda}^K(E) - \delta_{\beta,i}\delta_{\Lambda,\Lambda'}]|^2, \quad (16)$$

where $(2L_i+1)$ is the degeneracy of the initial state.

IV. RESULTS AND DISCUSSIONS

The total electron-transfer cross section is shown in Fig. 4 and compared with the previous theoretical calculations [5,3,6]. Up to 2.5 eV/amu the present results were obtained using the quantum-mechanical approach while at higher energy, the semiclassical eikonal method [24], which includes the Coriolis effects, has been used. Between 2.5 eV/amu and 3 eV/amu the agreement between the two approaches has been verified.

The agreement between the different theoretical total cross sections is only qualitative. Below 0.2 eV/amu, three quantum-mechanical results, two close-coupling [5,3] and the present time-dependent values, can be compared. Although the minimum of the total cross section can be found

for the three calculations around the same energy, the value of Opradolce *et al.* is about one order of magnitude higher than the two other results. The agreement between the present paper and the values of Stancil *et al.* is better. The increase of the cross section above 0.2 eV/amu, is very steep in the present paper and the maximum around 1.0 eV/amu culminates above the other values. When compared to the semiclassical calculation of Bacchus-Montabonel and Ceyz-

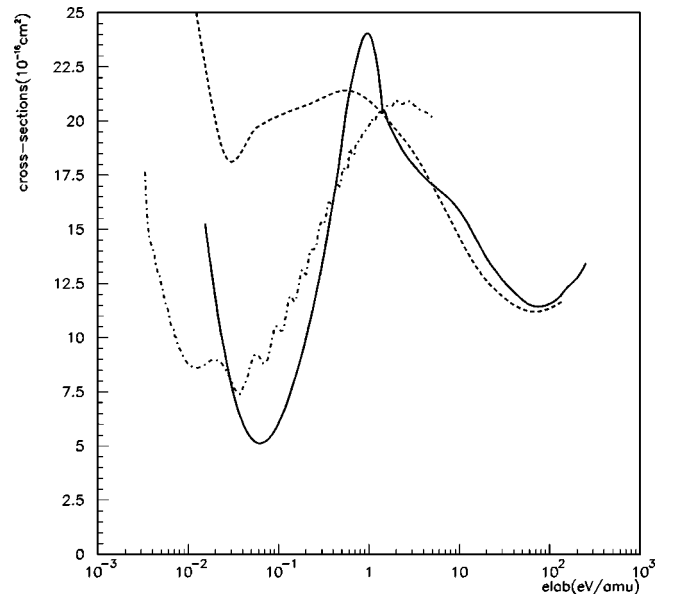


FIG. 4. Total electron-transfer cross section for the $\text{Si}^{4+} + \text{He}$ collision system: this paper, full curve; Opradolce *et al.* [5], long-dashed curve; and Stancil *et al.* [3], dash-dotted line.

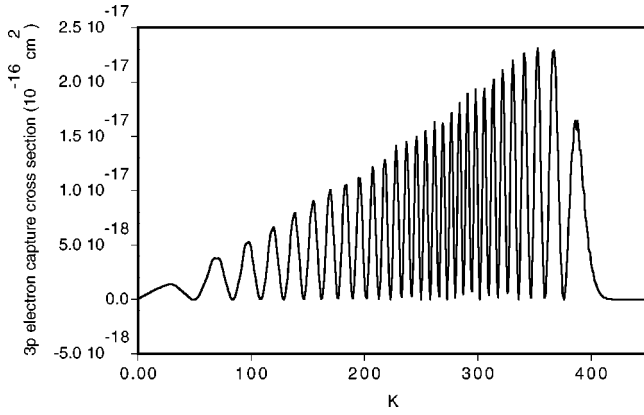


FIG. 5. Partial-wave contribution to the $3p\ ^1\Sigma^+$ state electron capture cross section in function of the total angular momentum K for a relative kinetic energy in the laboratory frame of 1.62 eV/amu.

eriat the agreement between the quantum-mechanical results of Stancil *et al.* and the results of the present paper is good. However, no resonance feature has been observed in the cross section in the two last calculations.

The oscillatory behavior of the total electron-transfer cross section found by Stancil *et al.* is confirmed in the present calculation. However, the local peaks in the cross section depend strongly on the wave-packet parameters. Therefore, the present total cross section is drawn without oscillatory structure. This oscillatory behavior can be understood by examing the partial cross section for the $3p\ ^1\Sigma^+$ channel at energy below 4 eV/amu. In this range of energy, the typical oscillations of the two states crossing partial cross section present a maximum for a partial wave below the cutoff value as shown in Fig. 5. When summed over all partial waves, a residual oscillatory structure is present in the cross section [25]. At this low energy, the $3s\ ^1\Sigma^+$ reactive channel is negligible and the behavior of the cross section

TABLE II. State-selective and total electron-transfer cross sections from the semiclassical eikonal calculation in 10^{-16} cm^2 .

E (eV/amu)	$\sigma_{3p\ ^1\Sigma^+}$	$\sigma_{3p\ ^1\Pi^+}$	$\sigma_{3s\ ^1\Sigma^+}$	σ_{Total}
2.262	18.706	1.215	$0.565 \cdot 10^{-4}$	19.921
2.505	17.283	1.194	$0.932 \cdot 10^{-4}$	18.477
3.032	17.720	1.291	$0.212 \cdot 10^{-3}$	19.263
3.607	16.367	1.280	$0.412 \cdot 10^{-3}$	17.647
4.234	17.670	1.315	$0.104 \cdot 10^{-2}$	18.986
4.910	16.960	1.314	$0.173 \cdot 10^{-2}$	18.276
5.637	16.261	1.375	$0.239 \cdot 10^{-2}$	17.638
10.024	14.569	1.274	$0.195 \cdot 10^{-1}$	15.862
22.550	11.829	1.331	0.180	13.340
40.000	9.919	1.508	0.683	12.110
62.500	8.777	1.632	1.079	11.489
90.000	7.920	1.787	1.779	11.486
122.857	7.392	1.959	2.451	11.802
160.357	7.125	2.088	3.150	12.363
202.857	6.802	2.222	3.758	12.782
250.536	6.720	2.398	4.306	13.424

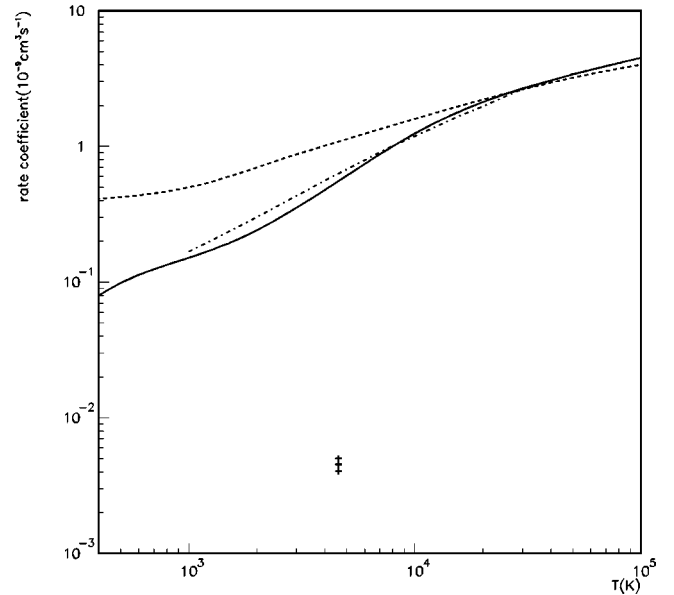


FIG. 6. Rate constant for the electron transfer to Si^{4+} ions from He: this paper, full curve; Opradolce *et al.* [5], long broken curve; and Stancil *et al.* [3], dash-dotted line. The experimental point of Fang and Kwong [1] is also given.

can be explained with a simple Landau-Zenner-Stueckelberg model [26].

Above 2.5 eV/amu, the semiclassical calculation included the Coriolis couplings, which therefore open the $3p\ ^1\Pi^+$ channel. In Table II, the cross sections to the $3p\ ^1\Sigma^+$, $3p\ ^1\Pi^+$, and $3s\ ^1\Sigma^+$ states are given. The table shows the increase of the cross sections to the $3p\ ^1\Pi^+$ and $3s\ ^1\Sigma^+$ states with increasing energy. However, this increase does not compensate for the decrease of the cross section to the $3p\ ^1\Sigma^+$ and the total cross section decreases until 90.0 eV/amu.

The rate constant as a function of the temperature is calculated by averaging the total electron-transfer cross section over a Maxwell-Boltzmann velocity distribution. The comparison between the present result and the previous theoretical values is done in Fig. 6. The experimental point obtained by Fang and Kwong [1] is also given. The present calculation shows that the value of the rate constant at low temperature depends dramatically on the behavior of the cross section near the threshold. The differences of behavior of the theoretical cross sections are clearly responsible for the discrepancies between the rate constants below 7×10^3 K. The present total electron-transfer cross section shows an increase near threshold in a rather similar way as in the calculation of Stancil *et al.*, giving rise to very similar behavior for the rate constant. The difference between the rate constant of Opradolce *et al.*, and the present one for a temperature of 4×10^2 K reflects the much higher value of the cross section at low energy obtained by the former. Finally, the only way to come close to the experimental value of Fang and Kwong is to artificially make the cross section tend to zero at low energy. Indeed, if a lower intergration limit of 0.2 eV/amu is taken, the evaluation of the rate constant using our cross section is in perfect agreement with the experimen-

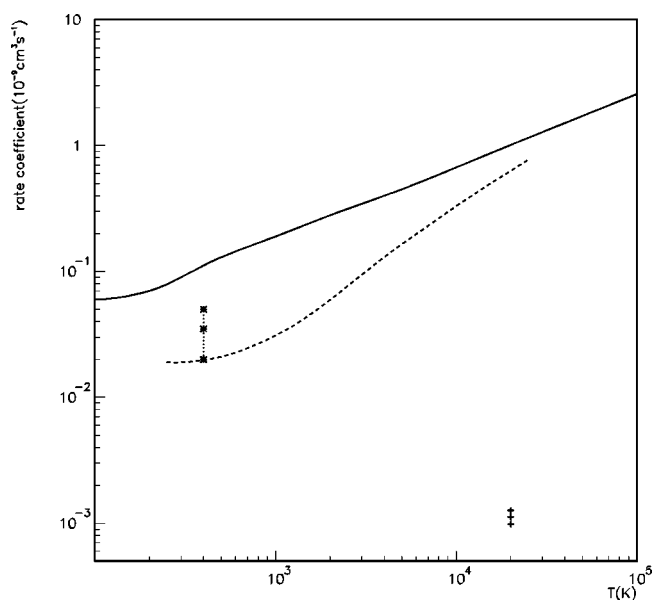


FIG. 7. Rate constant for the electron transfer to O^{2+} ions from He: Gargaud *et al.* [25] (full curve), and Butler *et al.* [27] (long-broken curve). The experimental points of Johnsen and Biondi [30] (star) and of Kwong and Fang [28,29] (cross) are also shown.

tal value. However, it is important to ask if the measurement of Fang and Kwong obtained using an ion trap with cylindrical symmetry can be compared with a calculation based on the use of a Maxwell-Boltzmann distribution. Moreover, the accuracy of the determination of the temperature of the ions in the presence of neutral atoms of helium can be questioned. The discrepancy between theoretical results [27,25] and the measurements of Fang and Kwong [28,29] occurs nearly in the same terms for the collisional system $O^{2+} + He$ as shown in Fig. 7. In this case, the experimental value [30] performed using drift tube techniques lies one order of magnitude above the result of Fang and Kwong but is a factor of 2 smaller than the quantum-mechanical calculation.

At high temperature, the rate constant seems to converge to the same value. All the theoretical calculations show the

same behavior independently of the details of the total cross sections, which can be very different from one calculation to another. Moreover, the upper integration limit is not a critical parameter in the evaluation of the rate constant.

V. CONCLUSIONS

The time-dependent wave-packet method has been applied to the calculation of electron-transfer cross section for the collisional system $Si^{4+} + He$ up to 2.5 eV/amu. For energy above this point, the calculations have been performed using a semiclassical eikonal approach, which includes Coriolis couplings. The range of energy cover by the present paper goes from 10^{-2} to 10^2 eV/amu.

The time-dependent approach have been applied in the diabatic representation using the split-operator technique and in the adiabatic representation using the Chebyshev method. Both results give the same result for the collision parameters assessing the accuracy of the numerical procedure.

The calculation of the rate constant for the electron-transfer reaction confirms the order of magnitude of the theoretical values. The disagreement observed previously with the experimental work of Fang and Kwong [1] is still unresolved. Nevertheless, the importance of the behavior of the total cross section at very low energy has been pointed out. At this point of view, a state-of-the-art cross beam experiment allowing for a experimental determination of the total cross section at very low energy could be an appropriate way to resolve the conflict between theory and experiment.

ACKNOWLEDGMENTS

The authors are very grateful to Dr. T. Bastin for helpful discussions. The research contribution of N.V. was supported by the Belgian National Fund for Scientific Research (FRFC Conventions). M.D.L. and E.B. acknowledge the financial support of the Communauté Française de Belgique (Actions de Recherche Concertées). N.V. and M.C.B.M. benefit from the cooperation project CNRS/CGRI-FNRS (No. 8057).

-
- [1] Z. Fang and V. H. S. Kwong, *Phys. Rev. A* **59**, 342 (1999).
 [2] D. R. Bates and B. L. Moiseiwitch, *Proc. Phys. Soc. London, Sect. A* **67**, 540 (1954).
 [3] P. C. Stancil, B. Zygelman, N. J. Clarke, and D. L. Cooper, *Phys. Rev. A* **55**, 1064 (1997).
 [4] E. Butler and A. Dalgarno, *Astrophys. J.* **241**, 838 (1980).
 [5] L. Opradolce, R. Mc Carroll, and P. Valiron, *Astron. Astrophys.* **148**, 229 (1985).
 [6] M.-C. Bacchus-Montabonel and P. Ceyzeriat, *Phys. Rev. A* **58**, 1162 (1998).
 [7] N. J. Clarke and D. L. Cooper, *J. Chem. Soc., Faraday Trans.* **94**, 3295 (1998).
 [8] N. Vaeck, M. Desouter-Lecomte, and J. Liévin, *J. Phys. B* **32**, 409 (1999).
 [9] MOLPRO (version 98.1) is a package of *ab initio* programs written by H.-J. Werner and P. Knowles, with contributions from J. Almlöf, R. D. Amos, M. J. O. Deegan, S. T. Elbert, C. Hampel, W. Meyer, K. Peterson, R. Pitzer, A. J. Stone, P. R. Taylor, and R. Lindh.
 [10] P. J. Hay and W. R. Wadt, *J. Chem. Phys.* **82**, 270 (1985).
 [11] A. D. McLean and G. S. Chandler, *J. Chem. Phys.* **72**, 5639 (1980).
 [12] P. Honvault, M. C. Bacchus-Montabonel, M. Gargaud, and R. McCarroll, *Chem. Phys.* **238**, 401 (1998).
 [13] T. H. Dunning, *J. Chem. Phys.* **90**, 1007 (1989).
 [14] D. E. Woon and T. H. Dunning, *J. Chem. Phys.* **100**, 2975 (1994).
 [15] H.-J. Werner and P. J. Knowles, *J. Chem. Phys.* **82**, 5053 (1985).
 [16] P. J. Knowles and H.-J. Werner, *Chem. Phys. Lett.* **115**, 259 (1985).

- [17] G. Parlant and D. R. Yarkony, *Int. J. Quantum Chem., Symp.* **26**, 737 (1992).
- [18] B. H. Lengsfeld III and D. R. Yarkony, *Adv. Chem. Phys.* **82**, 1 (1991).
- [19] M. D. Feit, J. A. Fleck, Jr., and A. Steiger, *J. Comput. Phys.* **47**, 412 (1982).
- [20] J. Alvarellos and H. Metiu, *J. Chem. Phys.* **88**, 4957 (1988).
- [21] H. Tal-Ezer and R. Kosloff, *J. Chem. Phys.* **81**, 3967 (1984).
- [22] B. Zygelman, D. L. Cooper, M. J. Ford, A. Dalgarno, J. Gerratt, and M. Raimondi, *Phys. Rev. A* **46**, 3846 (1992).
- [23] B. Zygelman, P. C. Stancil, N. J. Clarke, and D. L. Cooper, *Phys. Rev. A* **56**, 457 (1997).
- [24] R. J. Allan, C. Courbin, P. Salas, and P. Wahnon, *J. Phys. B* **23**, L461 (1990).
- [25] M. Gargaud, M. C. Bacchus-Montabonel, and R. McCarroll, *J. Chem. Phys.* **99**, 4495 (1993).
- [26] S. D. Augustin, W. H. Miller, P. K. Pearson, and H. F. Schaefer III, *J. Chem. Phys.* **58**, 2845 (1973).
- [27] S. E. Butler, T. G. Heil, and A. Dalgarno, *J. Chem. Phys.* **80**, 4986 (1984).
- [28] V. H. S. Kwong and Z. Fang, *Phys. Rev. Lett.* **71**, 4127 (1993).
- [29] Z. Fang and V. H. S. Kwong, *Phys. Rev. A* **51**, 1321 (1995).
- [30] R. Johnsen and M. A. Biondi, *J. Chem. Phys.* **74**, 305 (1981).